Ceramics International xxx (xxxx) xxx

Contents lists available at ScienceDirect

Ceramics International

journal homepage: www.elsevier.com/locate/ceramint

High-entropy $Mg_{1.8}R_{0.2}Al_4Si_5O_{18}$ (R = Ni, Co, Zn, Cu, Mn) cordierite ceramics: Influence of octahedral distortion and electronegativity mismatch on the microwave dielectric properties

Yang Yao [a,1], Lin Cao [a,1], Haoyue Yang [a], Raz Muhammad [b,**], Yingjie Ren [c], Xinjiang Luo [a], Fayaz Hussain [d], Bing Liu [a], Minmin Mao [a], Hadi Barzegar Bafrooei [a,f], Ehsan Taheri-Nassaj [e], Kaixin Song [a,*]

[a] College of Electronics Information, Hangzhou Dianzi University, Hangzhou, 310018, China
[b] Department of Physics, Abdul Wali Khan University Mardan, Garden Campus, Mardan, 23200, Khyber Pakhtunkhwa, Pakistan
[c] Institute of Communication Materials, Zhejiang Wazam New Materials Co., Ltd., Hangzhou, 311121, China
[d] Department of Materials Engineering, NED University of Engineering and Technology, Main University Road, Karachi, 75279, Pakistan
[e] Department of Materials Engineering, Faculty of Engineering, Tarbiat Modares University, Tehran, 14115-143, Iran
[f] Department of Materials Science and Engineering, School of Engineering, Meybod University, Yazd, 89616-99557, Iran

ARTICLE INFO

Handling Editor: Dr P. Vincenzini

Keywords:
Cordierite
High-entropy ceramic
Cation disorder
Electronegativity

ABSTRACT

In this study, high-entropy $Mg_{1.8}R_{0.2}Al_4Si_5O_{18}$ (R=Ni, $Ni_{1/2}Co_{1/2}$, $Ni_{1/3}Co_{1/3}Zn_{1/3}$, $Ni_{1/4}Co_{1/4}Zn_{1/4}Cu_{1/4}$, $Ni_{1/5}Co_{1/5}Zn_{1/5}Cu_{1/5}Mn_{1/5}$) cordierite ceramics based on equimolar ratios were designed and synthesized through the solid-state reaction technique at high temperatures. The effect of various R-ionic substitutions at the octahedral site and their relationship with ionic polarization, chemical bonding, and configurational entropy were explored. These factors have greatly affected the microwave dielectric properties of $Mg_{1.8}R_{0.2}Al_4Si_5O_{18}$ ceramics. The presence of cation radius mismatch and electronegativity mismatch at [MgO_6]-octahedron lattice sites revealed lattice distortion resulting from multiple cation substitutions. As the entropy values increased, the temperature stability of microwave dielectric properties of $Mg_{1.8}R_{0.2}Al_4Si_5O_{18}$ ceramics improved. For R=$Ni_{1/2}Co_{1/2}$, a higher $Q\times f$ of approximately 73,658 GHz @ 13 GHz, with ε_r ~4.44 and τ_f ~ −23.9 ppm/°C was obtained. In the case of R=$Ni_{1/5}Co_{1/5}Zn_{1/5}Cu_{1/5}Mn_{1/5}$, a near zero τ_f (−10.7 ppm/°C), ε_r = 4.68 and $Q\times f$ = 35,478 GHz @13 GHz were achieved, making it potentially suitable for practical applications.

1. Introduction

The demand for improved performance microwave dielectric ceramics is growing due to the rapid development of 5G/6G communication technologies, offering higher capacity and lower latency. Generally, low relative dielectric constant (ε_r), low dielectric loss/high quality factor ($Q\times f$), and near zero temperature coefficient of resonant frequency (τ_f) are requirements for dielectric materials to be used in high-frequency applications [1–5]. Silicates, tungstates, phosphates, borates, and molybdates are generally considered to have low ε_r and low dielectric losses [6–14]. However, their poor thermal stability of resonance frequency renders them used in practical applications.

The high-entropy process represents a breakthrough in conventional material design concepts and opens up possibilities for new material development, which is a multicomponent material composed of nearly equal or equiatomic proportions of multiple cations at the same lattice site [15–19]. There is a certain relationship between the entropy (S) and enthalpy (H) of a system, which is expressed by the Gibbs free energy (G) formula:

$$G = H - TS \quad (1)$$

An increase in entropy in the system will result in a decrease in the Gibbs free energy, leading to a more stable crystal structure [20,21]. The crystal lattice of high-entropy ceramics can be divided into two parts.

* Corresponding author.
** Corresponding author.
E-mail addresses: raz@awkum.edu.pk (R. Muhammad), kxsong@hdu.edu.cn (K. Song).
[1] These authors equally contributed to this work.

https://doi.org/10.1016/j.ceramint.2024.02.215
Received 13 November 2023; Received in revised form 28 January 2024; Accepted 17 February 2024
Available online 19 February 2024

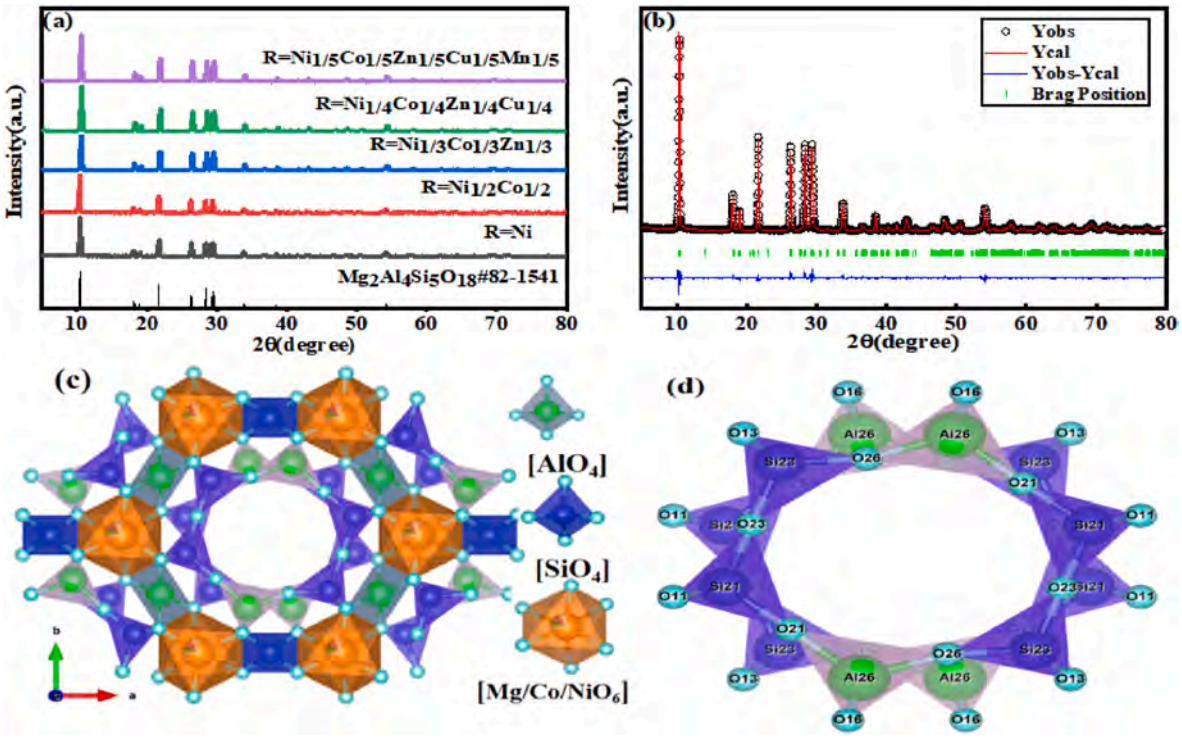

Fig. 1. (a) XRD patterns of $Mg_{1.8}R_{0.2}Al_4Si_5O_{18}$ ceramic at the optimal sintering temperature as a function of R, (b) observed, calculated, and difference in the XRD pattern of $Mg_{1.8}R_{0.2}Al_4Si_5O_{18}$ (R═$Ni_{1/5}Co_{1/5}Zn_{1/5}Cu_{1/5}Mn_{1/5}$), (c) the sketch of $Mg_{1.8}R_{0.2}Al_4Si_5O_{18}$ crystal structure, and (d) the sketch of $[(Si_4Al_{12})O_{18}]$ ring.

One part is the anion sublattice, which is prone to being occupied by vacancies or anionic species. The other part is the metal cation sublattice, which is susceptible to being randomly occupied by multiple metal atoms.

Currently, various types of high-entropy rock salt [22], fluorite [23], perovskite [24], spinel [25] and corundum [26] structures, etc. have been developed. Gild et al. [23] developed single-phase fluorite-type high-entropy compositions based on $(Hf_{0.25}Zr_{0.25}Ce_{0.25}Y_{0.25})O_{2-\delta}$ ceramics doped with different elements and achieved low thermal conductivity, low electrical conductivity, and high hardness. Zhou et al. [27] synthesized a group of $Ba(Zr_{0.2}Ti_{0.2}Sn_{0.2}Hf_{0.2}Me_{0.2})O_3$ perovskite-type high-entropy ceramics (Me = Y^{3+}, Nb^{5+}, Ta^{5+}, V^{5+}, Mo^{6+}, W^{6+}), which exhibited excellent temperature stability in the range of 25–200 °C. The high entropy A_2BO_4 compounds have also been studied with a low dielectric constant and olivine structure such as $LiABO_4$ (A = Mg, Zn, Ca, Ln; B═Si, Ge) [28–35]. Until now, there have been no relevant reports on high-entropy cordierite ceramics. Ohsato et al. [36] reported $Q\times f$ = 99,100 GHz for the $(Mg_{1-x}Ni_x)_2Al_4Si_5O_{18}$ (x = 0.1) ceramics. The group has previously investigated the dependence of the substitution of R═Mg, Ca, Sr, Ba, Mn, Co, Ni, Cu, Zn on the microwave dielectric properties of $Mg_{1.8}R_{0.2}Al_4Si_5O_{18}$. Their findings revealed that the $Q\times f$ value decreased with the substitution of Ni, Co, Mn, Zn, and Cu. Notably, $Mg_{1.8}Ni_{0.2}Al_4Si_5O_{18}$ demonstrated the best performance, with a $Q \times f$ value of 61,880 GHz, ε_r = 4.53, and τ_f = −32 ppm/°C [37].

In this study, the strategy of high entropy of $Mg_{1.8}R_{0.2}Al_4Si_5O_{18}$ cordierite ceramic with R═Ni, $Ni_{1/2}Co_{1/2}$, $Ni_{1/3}Co_{1/3}Zn_{1/3}$, $Ni_{1/4}Co_{1/4}Zn_{1/4}Cu_{1/4}$, $Ni_{1/5}Co_{1/5}Zn_{1/5}Cu_{1/5}Mn_{1/5}$ was adopted which successfully resulted into enhanced thermal stability of the microwave dielectric properties. The effect of various R-ionic substitutions at the octahedral $[MgO_6]$ site on the ionic polarization, chemical bonding, and configurational entropy was explored which ultimately affected the microwave dielectric characteristics of $Mg_{1.8}R_{0.2}Al_4Si_5O_{18}$ ceramics.

2. Experimental procedure

Reagent grade MgO, Al_2O_3, SiO_2, NiO, CoO, ZnO, CuO, and $MnCO_3$ (all from Aladdin company, China) were used for the synthesis of $Mg_{1.8}R_{0.2}Al_4Si_5O_{18}$ (R═Ni, $Ni_{1/2}Co_{1/2}$, $Ni_{1/3}Co_{1/3}Zn_{1/3}$, $Ni_{1/4}Co_{1/4}Zn_{1/4}Cu_{1/4}$, $Ni_{1/5}Co_{1/5}Zn_{1/5}Cu_{1/5}Mn_{1/5}$) ceramics. After weighing the precursors as per stoichiometric ratios of the compositions, the batch compositions were ball-milled for 24 h in ethanol, using zirconia balls as a grinding media. The slurry was dried at 80 °C and then sieved. The sieved powders were calcined at 1200 °C/4 h, at a ramp rate of 4 °C/min in air. The calcined powders were reground and pressed into cylindrical pellets with a diameter of 12 mm and thickness of 7 mm, at a pressure of 100 MPa. Finally, the green pellets were sintered at 1400–1430 °C/4 h.

The Archimedes method was employed to measure the bulk density of sintered pellets. The crystal structure was identified using an X-ray diffractometer (XRD: RIGAKU D/max 2550/PC, Rigaku Co., Japan) with Cu-Kα radiation. The microstructure was examined using a scanning electron microscope (SEM, S-3400 Hitachi, Japan). A Keysight (N5234B) vector network analyzer using the TE01δ mode was used to measure the microwave dielectric properties (ε_r and $Q\times f$) of the sintered ceramics. The following formula was used to measure the τ_f value:

$$\tau_f = \frac{f_{85} - f_{25}}{f_{25} \times (85 - 25)} \times 10^6 ppm \Big/ ^{\circ}C \quad (2)$$

The resonant frequencies at 85 and 25 °C, respectively, are denoted by f_{85} and f_{25}.

3. Results and discussions

Fig. 1(a) displays the X-ray diffraction (XRD) patterns of the high-entropy $Mg_{1.8}R_{0.2}Al_4Si_5O_{18}$ ceramics sintered at the optimal temperature. All the diffraction peaks correspond to the cordierite phase of $Mg_2Al_4Si_5O_{18}$ (JCPDS No. 82–1541, space group of *Cccm* (66)). Fig. 1(b) shows the fitted XRD pattern for $Mg_{1.8}R_{0.2}Al_4Si_5O_{18}$ (R═$Ni_{1/5}Co_{1/5}Zn_{1/5}Cu_{1/5}Mn_{1/5}$) ceramics. The fitted XRD patterns for all components are

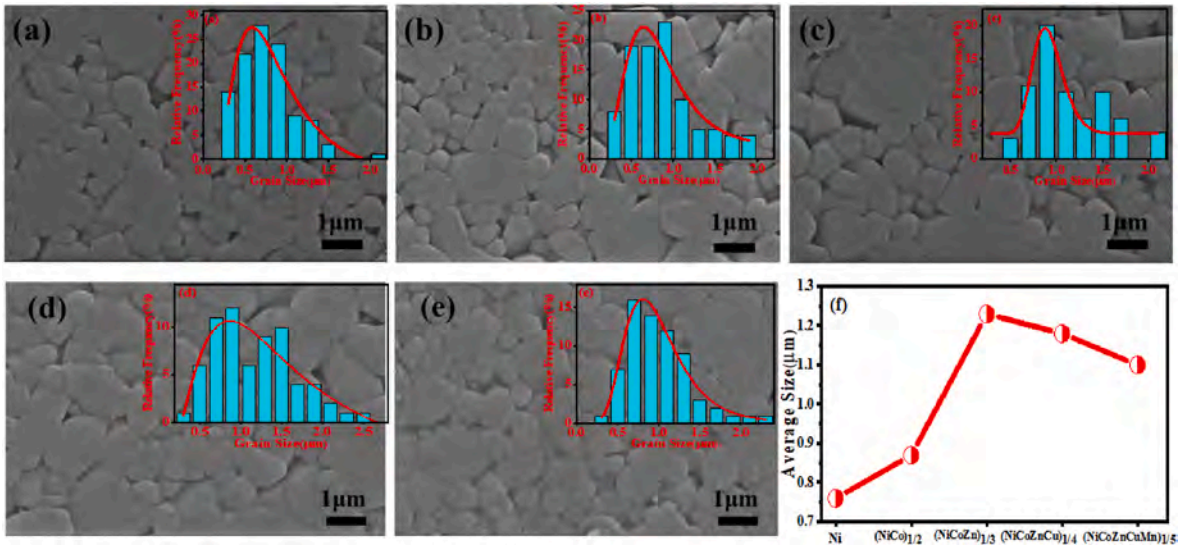

Fig. 2. SEM images of $Mg_{1.8}R_{0.2}Al_4Si_5O_{18}$ ceramics with different R = (a) Ni, (b) $Ni_{1/2}Co_{1/2}$, (c) $Ni_{1/3}Co_{1/3}Zn_{1/3}$, (d) $Ni_{1/4}Co_{1/4}Zn_{1/4}Cu_{1/4}$, (e) $Ni_{1/5}Co_{1/5}Zn_{1/5}Cu_{1/5}Mn_{1/5}$), and (f) average grain size distribution of $Mg_{1.8}R_{0.2}Al_4Si_5O_{18}$ high-entropy ceramics.

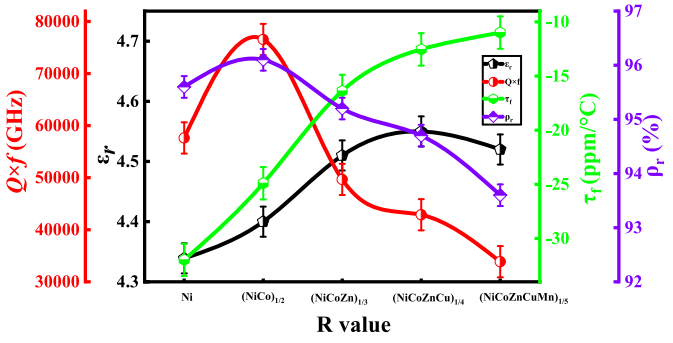

Fig. 3. Variation in ε_r, $Q\times f$ value, τ_f, and relative density of $Mg_{1.8}R_{0.2}Al_4Si_5O_{18}$ high-entropy ceramics.

shown in Fig. S1(a)–(e) (SI), and the refined lattice parameters are summarized in Table S1 (SI). The values of refinement factors show the reliability of fitting. Fig. 1(c) shows the crystal structure of $Mg_{1.8}R_{0.2}Al_4Si_5O_{18}$ (R═$Ni_{1/5}Co_{1/5}Zn_{1/5}Cu_{1/5}Mn_{1/5}$) ceramics, with Ni, Co, Zn, Cu, and Mn ions occupying the A-site. The presence of multiple cations leads to structural complexity. Fig. 1(d) shows the six-membered ring of $[Si_4Al_2)O_{18}]$, which is composed of six tetrahedrally coordinated oxygen atoms linked to silicon (Si) and aluminum (Al) cations.

Fig. 2 displays the scanning electron micrographs of the thermally etched surfaces of the high-entropy $Mg_{1.8}R_{0.2}Al_4Si_5O_{18}$ ceramics sintered at the optimal sintering temperature. All the samples exhibit a relatively dense microstructure. Fig. 2(f) shows that the average grain size of the samples initially increased from 0.7 to 1.3 μm. Interestingly, this trend demonstrates a continuous increase followed by a subsequent decrease. This phenomenon could be attributed to the variation in ion radii of the dopant(s) resulting from the incorporation of Ni, Co, Zn, Cu, and Mn. The radius of these dopant ions initially increases and then decreases, influencing the grain growth during sintering. Another reason may be the inhibition of grain growth due to copper substitution.

Fig. 3 shows the relative densities and microwave dielectric properties of $Mg_{1.8}R_{0.2}Al_4Si_5O_{18}$ high-entropy ceramics as a function of R. The sintering of the ceramic gradually deteriorates, resulting in a decrease in relative density. ε_r initially increases and then slightly decreases with an increase in the number of doped ions. The change in $Q\times f$ value shows a similar trend to that of relative density, reaching its maximum value after 1/2Ni −1/2Co co-doped $Mg_{1.8}R_{0.2}Al_4Si_5O_{18}$ with $\varepsilon_r = 4.4$, $Q\times f = 73658$ GHz, and $\tau_f = -23.9$ ppm/°C. When R═$Ni_{1/5}Co_{1/5}Zn_{1/5}Cu_{1/5}Mn_{1/5}$, the ceramic exhibits the highest entropy value, possessing $\varepsilon_r = 4.68$, $Q\times f = 33{,}875$ GHz, and $\tau_f = -10.98$ ppm/°C. The high entropy strategy improved the temperature stability and decreased the $Q\times f$ value of cordierite ceramic.

The ε_r is mainly influenced by the ionic nature of chemical bonds and the porosity of the material [38]. Fig. 4 (a) illustrates the actual

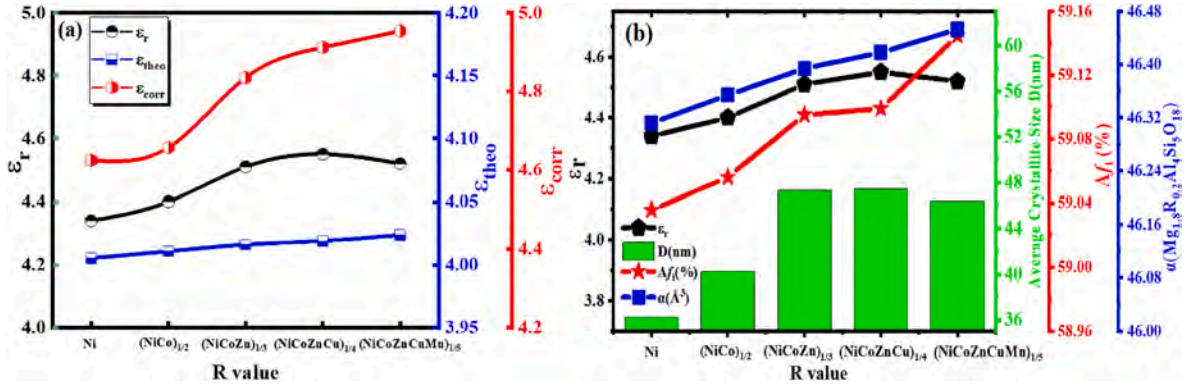

Fig. 4. (a) Variation of the ε_r, ε_{theo}, and ε_{corr}, and (b) the dependence of ε_r on grain sizes, polarizability (α), and average ionicity (Af_i%) of high-entropy ceramics as a function of element numbers.

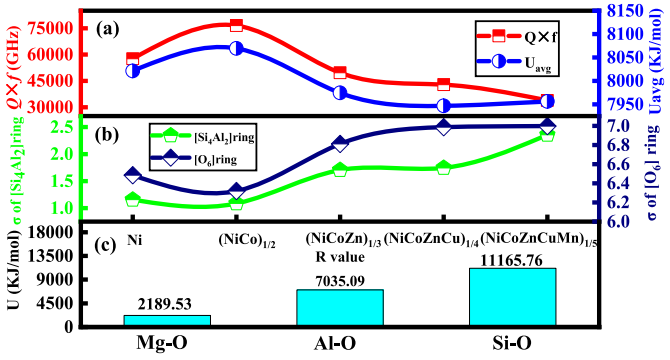

Fig. 5. (a) $Q\times f$ and U_{ave} versus R in $Mg_{1.8}R_{0.2}Al_4Si_5O_{18}$ ceramics (R=Ni, $Ni_{1/2}Co_{1/2}$, $Ni_{1/3}Co_{1/3}Zn_{1/3}$, $Ni_{1/4}Co_{1/4}Zn_{1/4}Cu_{1/4}$, $Ni_{1/5}Co_{1/5}Zn_{1/5}Cu_{1/5}Mn_{1/5}$), (b) σ of the $[Si_4Al_2]$ and $[O_6]$ hexagonal rings, and (c) the average lattice energy of Mg–O, Al–O, and Si–O bonds.

dielectric constant (ε_r), theoretical dielectric constant (ε_{theo}), and the dielectric constant after pore correction (ε_{corr}) for $Mg_{1.8}R_{0.2}Al_4Si_5O_{18}$ high-entropy ceramics, showing an increase with an increase in the number of dopants. However, when R=$Ni_{1/5}Co_{1/5}Zn_{1/5}Cu_{1/5}Mn_{1/5}$, the slope of ε_r is lower than the slopes of ε_{theo} and ε_{corr}, and ε_r begins to decrease, which is opposite to the calculated ε_{theo} and ε_{corr}. Fig. 4(b) shows that ε_r, molecular polarizability (α) and average ionicity (Af_i) have a direct relationship. However, the non-linearity as a function number of dopants/concentration may be correlated with the change in the crystallite size of the $Mg_{1.8}R_{0.2}Al_4Si_5O_{18}$ high entropy ceramics.

The average lattice energy (U_{avg}) was calculated from the refined bond lengths and bond angles using complex chemical bonding theory. The $Q\times f$ was found to decrease with a decrease in average lattice energy, Fig. 5(a). Compared with Al–O and Mg–O, the lattice energy (U) of Si–O is the largest, indicating that it dominates the $Q\times f$ value (Fig. 5(c)). $Q\times f$ values are also related to the symmetry of the $[Si_4Al_2]$ and $[O_6]$ hexagonal rings in the cordierite crystal structure [39,40]. Therefore, the standard deviation value (σ) of the two hexagonal rings of $Mg_{1.8}R_{0.2}Al_4Si_5O_{18}$ high-entropy ceramic, corresponding to the symmetry of the two $[Si_4Al_2]$ and $[O_6]$ hexagonal rings are calculated using eqn. (3):

$$\sigma=\sqrt{\frac{\left[(A_1-120^\circ)^2+(A_2-120^\circ)^2+(A_3-120^\circ)^2\right]\times 2}{6}} \tag{3}$$

In the formula, the degrees of bond angles Si(2)-Al(2)-Si(3), Si(3)-Si(2)-Al(2), Si(2)-Si(3)-Al(2), Si(2)-Si(3)-Al(2) are represented in the hexagonal ring of $[Si_4Al_2]$, and the degrees of bond angles O(5)-O(4)-O(6), O(4)-O(6)-O(5), O(6)-O(5)-O(4) are represented in the hexagonal ring of $[O_6]$. σ shows an inverse relationship with the $Q\times f$, as seen in Fig. 5 (b).

Fig. 6(a) shows that τ_f is strongly dependent on the average bond energy of Al–O, the radius of the dopants, and distortion of the Mg/RO_6 octahedra in $Mg_{1.8}R_{0.2}Al_4Si_5O_{18}$ high-entropy ceramics. Octahedral distortion can be calculated from the bond lengths that are longest (d_{max}), shortest (d_{min}), and average (d_{avg}) of the octahedron using eqn. (4).

$$\Delta_{octa.}=\frac{d_{max}-d_{min}}{d_{avg}} \tag{4}$$

The distorting structure of $[Mg_{0.8}R_{0.2})O_6]$ octahedra is shown in Fig. 6(b). The distortion of the $[(Mg_{0.8}R_{0.2})O_6]$ octahedra decreases, accompanied by an increase in the average bond energy of the Al–O bonds ($E_{(Al-O)}$), which in turn increase τ_f from −33 to −12 ppm/°C. However, when R=$Ni_{1/5}Co_{1/5}Zn_{1/5}Cu_{1/5}Mn_{1/5}$, the distortion of the octahedra increases. This may be due to the smaller radius of Mn ions doping, causing a significant difference in size between $(Ni_{1/5}Co_{1/5}Zn_{1/5}Cu_{1/5}Mn_{1/5})^{2+}$ (0.72 Å) and Mg^{2+} (0.89 Å), leading to a larger distortion in the Mg–O octahedra.

The high entropy effect should lead to improved performance and easier formation of single-phase ceramics [16]. In equiatomic multi-component systems, the greater mixing enthalpy leads to a reduction in free energy. This makes it more feasible to achieve thermodynamically stable systems and easily form single-phase ceramics [41]. In cordierite ceramics, there is no data available to assess the entropy effect. The mixing entropy (S_{mix}) is calculated using eqn. 5. Only considering the disorder of Mg lattice sites, the Al/Si/O lattice sites do not contribute to the total mixing entropy. Therefore, the configurational entropy (S_{config}) of cordierite ceramics can be calculated using eqn. 6.

$$\Delta S_{mix}=-R\left[\frac{h}{h+k+l+m}\sum_{i=1}^{N_h}x_i^h\ln\left(x_i^h\right)+\frac{k}{h+k+l+m}\sum_{i=1}^{N_k}x_i^k\ln\left(x_i^k\right)+\frac{l}{h+k+l+m}\sum_{i=1}^{N_l}x_i^l\ln\left(x_i^l\right)+\frac{m}{h+k+l+m}\sum_{i=1}^{N_m}x_i^m\ln\left(x_i^m\right)\right] \tag{5}$$

$$\Delta S_{config}=-R\left[2\left(\sum_{i=1}^{N_h}x_i^h\ln\left(x_i^h\right)\right)_{Mg-site}+4\left(\sum_{i=1}^{N_k}x_i^k\ln\left(x_i^k\right)\right)_{Al-site}+5\left(\sum_{i=1}^{N_l}x_i^l\ln\left(x_i^l\right)\right)_{Si-site}+18\left(\sum_{i=1}^{N_m}x_i^m\ln\left(x_i^m\right)\right)_{O-site}\right] \tag{6}$$

Here, h, k, l, and m represent the number of Mg, Al, Si, and O lattice sites in cordierite, respectively. R is the ideal gas constant. N_h, N_k, N_l, and N_m represent the number of element types in the h, k, l, and m lattice sites, respectively. x_i^h, x_i^k, x_i^l, and x_i^m represent the molar fractions of component i in the h, k, l, and m lattice sites, respectively.

The ability of single-phase formation of multi-component ceramics is related to structural deformation [16]. In this context, two parameters, namely, disorder of ionic radius (δ^r) and electronegativity mismatch (δ^χ) are used to explain the influence of effects of atomic properties, composition, and entropy on phase stability. The level of lattice distortion can be evaluated by considering δ^r and δ^χ of all the elements [42,43]. The atomic radius at the Mg lattice and electronegativity in cordierite can be calculated using the following formulas.

$$\delta^r_{Mg-site}=\sqrt{\sum_i c_i\left(1-\frac{r^i}{\bar{r}}\right)^2} \tag{7}$$

$$\bar{r}=\sum_i c_i r^i \tag{8}$$

$$\delta^\chi_{Mg-site}=\sqrt{\sum_i c_i\left(1-\frac{\chi^i}{\bar{\chi}}\right)^2} \tag{9}$$

$$\bar{\chi}=\sum_i c_i\left(1-\frac{\chi^i}{\bar{\chi}}\right) \tag{10}$$

C^i represents the molar fraction of the i-th component at the Mg lattice sites, while r^i and χ^i represent the radius and electronegativity of the i-th component at the Mg lattice sites. $\bar{r}$ and $\bar{\chi}$ represent the average

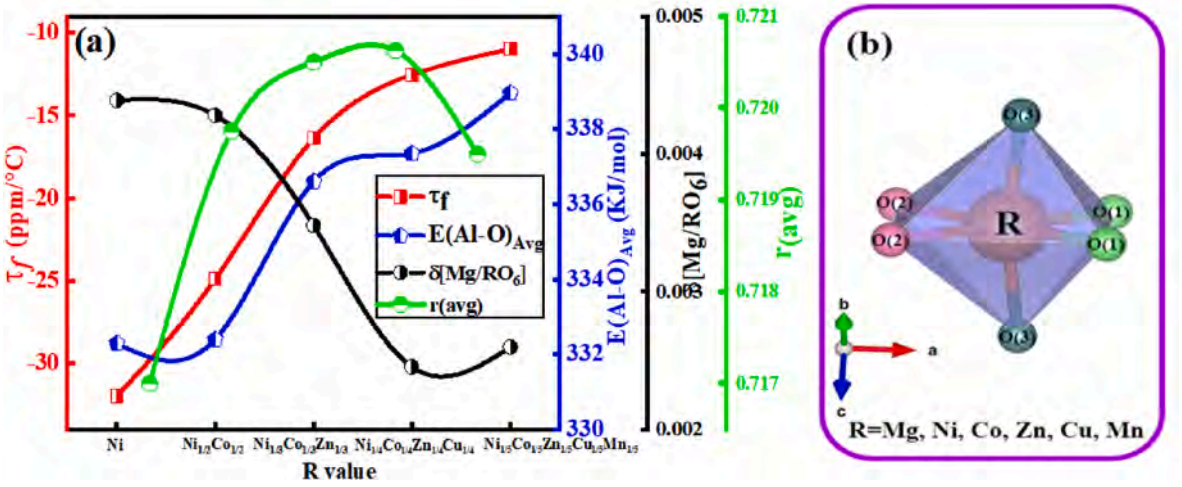

Fig. 6. (a) Variation in τ_f, average bond energy of Al–O bonds, distortion level of [Mg/RO_6] octahedra and ion radius of dopants, and (b) schematic representation of the BO_6 octahedra in $Mg_{1.8}R_{0.2}Al_4Si_5O_{18}$ high-entropy ceramics.

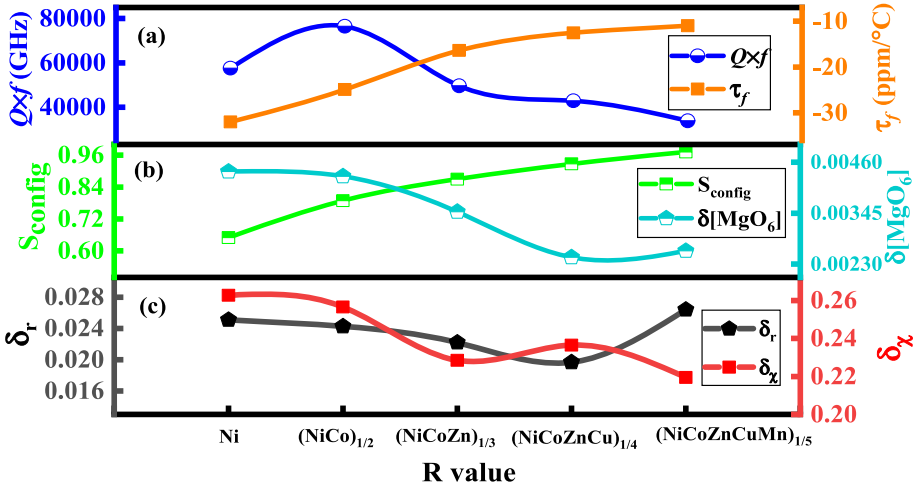

Fig. 7. (a) $Q\times f$ values and τ_f, (b) S_{config} and [MgO_6] octahedral distortion, and (c) δ^r and δ^χ at Mg lattice sites in $Mg_{1.8}R_{0.2}Al_4Si_5O_{18}$ high-entropy ceramics as a function of R=Ni, $Ni_{1/2}Co_{1/2}$, $Ni_{1/3}Co_{1/3}Zn_{1/3}$, $Ni_{1/4}Co_{1/4}Zn_{1/4}Cu_{1/4}$, $Ni_{1/5}Co_{1/5}Zn_{1/5}Cu_{1/5}Mn_{1/5}$.

radius and average electronegativity of multiple cations at the Mg lattice sites. $Q \times f$ value increases and τ_f value decreases with an increase in the entropy configuration, Fig. 7(a) and (b). Fig. 7(c) shows the decrease in both δ^r and δ^χ at Mg lattice sites which is favorable for the stability of the $Mg_{1.8}R_{0.2}Al_4Si_5O_{18}$ structure in high-entropy ceramics, resulting in reduced octahedral distortion, consistent with Fig. 7(b). The reduction of δ^r and δ^χ favors the reduction of octahedral distortion, resulting in an increased τ_f. Therefore, the distortion of [$(Mg_{0.8}R_{0.2})O_6$] octahedra in high-entropy ceramics shows a decreasing trend followed by a slight increase with the increase in configurational entropy.

4. Conclusions

In this work, high-entropy equimolar compositions of $Mg_{1.8}R_{0.2}Al_4Si_5O_{18}$ ceramics were synthesized using the solid-state reaction method. XRD and SEM analysis confirmed that all samples were single-phase ceramics, with an average grain size distribution from 0.7 μm to 1.3 μm and a relative density between 92% and 97%. The measured dielectric constant (ε_r) of the high-entropy ceramics increased from 4.3 to 4.5 with varying R, attributed to factors such as ceramic microcrystal size, polarizability, and chemical bond ionicity. However, there was a decrease in $Q\times f$ values from 76,539 GHz to 33,875 GHz. This decrease was primarily due to the reduction in lattice energy of Si–O bonds and the distortion of [Si_4Al_2] and [O_6] hexagonal rings, caused by multiple ionic replacements in the Mg site. Relative density also played a role. Conversely, the temperature coefficient (τ_f) increased from −31.97 ppm/°C to −10.98 ppm/°C. This increase was associated with the rise in configurational entropy (S_{config}), cation radius disorder (δr), electronegativity disorder (δχ), and the reduction of [MgO_6] octahedral distortion. These factors collectively contributed to a temperature coefficient closer to zero, enhancing the temperature stability of the ceramics. Notably, when R=$Ni_{1/5}Co_{1/5}Zn_{1/5}Cu_{1/5}Mn_{1/5}$, the temperature coefficient approaches zero, resulting in impressive microwave dielectric performance with $\varepsilon_r = 4.68$, $Q\times f = 33{,}875$ GHz, and $\tau_f = -10.98$ ppm/°C.

Declaration of competing interest

The authors declare that they have no known competing financial interests or personal relationships that could have appeared to influence the work reported in this paper.

Acknowledgments

This work was supported by the “Leading Geese” research and development planning project of the Department of Science and

Technology of Zhejiang province (No.2023C01183) and the Natural Science Foundation of China (Grant No.52161145401, 51672063).

Appendix A. Supplementary data

Supplementary data to this article can be found online at https://doi.org/10.1016/j.ceramint.2024.02.215.

References

[1] Z.Y. Xiu, M.M. Mao, Z.L. Lu, et al., High-Qf value and temperature stable Zn^{2+}-Mn^{4+} cooperated modified cordierite-based microwave and millimeter-wave dielectric ceramics, J. Eur. Ceram. Soc. 42 (2022) 5712–5717.
[2] W.C. Lou, K.X. Song, F. Hussain, et al., Bond characteristics and microwave dielectric properties of $(Li_{0.5}Ga_{0.5})^{2+}$ doped $Mg_2Al_4Si_5O_{18}$ ceramics, Ceram. Int. 46 (18) (2020).
[3] T. Joseph, M.T. Sebastian, Microwave dielectric properties of $(Sr_{1-x}A_x)_2(Zn_{1-x}B_x)Si_2O_7$ ceramics (A= Ca, Ba and B= Co, Mg, Mn, Ni), J. Am. Ceram. Soc. 93 (1) (2010) 147–154.
[4] F. Kamutzki, S. Schneider, J. Barowski, et al., Silicate dielectric ceramics for millimetre wave applications, J. Eur. Ceram. Soc. 41 (7) (2021) 3879–3894.
[5] W.C. Lou, M.M. Mao, K.X. Song, et al., Low permittivity cordierite-based microwave dielectric ceramics for 5G/6G telecommunications, J. Eur. Ceram. Soc. (6) (2022) 42.
[6] D. Zhou, L.X. Pang, D.W. Wang, et al., High quality factor, ultralow sintering temperature $Li_6B_4O_9$ microwave dielectric ceramics with ultralow density for antenna substrates, ACS Sustainable Chem. Eng. 6 (8) (2018) 11138–11143.
[7] L.X. Pang, D. Zhou, D.W. Wang, et al., Temperature stable $K_{0.5}(Nd_{1-x}Bi_x)_{0.5}MoO_4$ microwave dielectrics ceramics with ultra-low sintering temperature, J. Am. Ceram. Soc. 101 (5) (2018) 1806–1810.
[8] X.K. Lan, J. Li, Z.Y. Zou, et al., Lattice structure analysis and optimised microwave dielectric properties of $LiAl_{1-x}(Zn_{0.5}Si_{0.5})_xO_2$ solid solutions, J. Eur. Ceram. Soc. 39 (7) (2019) 2360–2364.
[9] J.B. Song, K.X. Song, J.S. Wei, et al., Ionic occupation, structures, and microwave dielectric properties of $Y_3MgAl_3SiO_{12}$ garnet-type ceramics, J. Am. Ceram. Soc. 101 (1) (2018) 244–251.
[10] L. Li, C.H. Liu, J.Y. Zhu, et al., B_2O_3-modified fused silica microwave dielectric materials with ultra-low dielectric constant, J. Eur. Ceram. Soc. 35 (6) (2015) 1799–1805.
[11] D. Zhou, C.A. Randall, L.X. Pang, et al., Microwave dielectric properties of Li_2WO_4 ceramic with ultra-low sintering temperature, J. Am. Ceram. Soc. 94 (2) (2011) 348–350.
[12] X. Zhou, L.T. Liu, J.J. Sun, et al., Effects of $(Mg_{1/3}Sb_{2/3})^{4+}$ substitution on the structure and microwave dielectric properties of $Ce_2Zr_3(MoO_4)_9$ ceramics, J. Adv. Ceram. 10 (2021) 778–789.
[13] C. Feng, X. Zhou, B.J. Tao, et al., Crystal structure and enhanced microwave dielectric properties of the $Ce_2[Zr_{1-x}(Al_{1/2}Ta_{1/2})_x]_3(MoO_4)_9$ ceramics at microwave frequency, J. Adv. Ceram. 11 (3) (2022) 392–402.
[14] H.R. Tian, J.J. Zheng, L.T. Liu, et al., Structure characteristics and microwave dielectric properties of $Pr_2(Zr_{1-x}Ti_x)_3(MoO_4)_9$ solid solution ceramic with a stable temperature coefficient, J. Mater. Sci. Technol. 116 (2022) 121–129.
[15] X.P. Wang, F.T. Fan, Resent development in high-entropy alloys and other high-entropy materials, J. Aeronautical Mater. 39 (6) (2019) 1–19.
[16] C.M. Rost, E. Sachet, T. Borman, et al., Entropy-stabilized oxides, Nat. Commun. 6 (1) (2015) 8485.
[17] R. Djenadic, A. Sarkar, O. Clemens, et al., Multicomponent equiatomic rare earth oxides, Mater. Res. Lett. 5 (2) (2017) 102–109.
[18] K. Chen, X. Pei, L. Tang, et al., A five-component entropy-stabilized fluorite oxide, J. Eur. Ceram. Soc. 38 (11) (2018) 4161–4164.
[19] S. Jiang, T. Hu, J. Gild, et al., A new class of high-entropy perovskite oxides, Scripta Mater. 142 (2018) 116–120.
[20] L. Backman, J. Gild, J. Luo, et al., Part I: theoretical predictions of preferential oxidation in refractory high entropy materials, Acta Mater. 197 (2020) 20–27.
[21] R. Feng, P.K. Liaw, M.C. Gao, et al., First-principles prediction of high-entropy-alloy stability, npj Comput. Mater. 3 (1) (2017) 50.
[22] B. Ye, T. Wen, M.C. Nguyen, et al., First-principles study, fabrication and characterization of $(Zr_{0.25}Nb_{0.25}Ti_{0.25}V_{0.25})C$ high-entropy ceramics, Acta Mater. 170 (2019) 15–23.
[23] J. Gild, M. Samiee, J.L. Braun, et al., High-entropy fluorite oxides, J. Eur. Ceram. Soc. 38 (10) (2018) 3578.
[24] S. Jiang, T. Hu, J. Gild, et al., A new class of high-entropy perovskite oxides, Scripta Mater. 142 (2018) 116–120.
[25] A. Mao, F. Quan, H.Z. Xiang, et al., Facile synthesis and ferrimagnetic property of spinel $(CoCrFeMnNi)_3O_4$ high-entropy oxide nanocrystalline powder, J. Mol. Struct. 1194 (2019) 11–18.
[26] S.J. McCormack, A. Navrotsky, Thermodynamics of high entropy oxides, Acta Mater. 202 (2021) 1–21.
[27] S.Y. Zhou, Y.P. Pu, Q.W. Zhang, et al., Microstructure and dielectric properties of high entropy Ba $(Zr_{0.2}Ti_{0.2}Sn_{0.2}Hf_{0.2}Me_{0.2})O_3$ perovskite oxides, Ceram. Int. 46 (6) (2020) 7430–7437.
[28] C. Oses, C. Toher, S. Curtarolo, et al., High-entropy ceramics, Nat. Rev. Mater. 5 (4) (2020) 295–309.
[29] K.X. Song, X.M. Chen, X.C. Fan, et al., Effects of Mg/Si ratio on microwave dielectric characteristics of forsterite ceramics, J. Am. Ceram. Soc. 90 (6) (2007) 1808–1811.
[30] J. Sugihara, K. Kakimoto, I. Kagomiya, et al., Microwave dielectric properties of porous Mg_2SiO_4 filling with TiO_2 prepared by a liquid phase deposition process, J. Eur. Ceram. Soc. 27 (8–9) (2007) 3105–3108.
[31] H.C. Xiang, C.C. Li, H. Jantunen, et al., Ultralow loss $CaMgGeO_4$ microwave dielectric ceramic and its chemical compatibility with silver electrodes for low-temperature cofired ceramic applications, ACS Sustain. Chem. Eng. 6 (5) (2018) 6458–6466.
[32] A. Rose, B. Masin, H. Sreemoolanadhan, et al., Synthesis and microwave dielectric studies of pure Li_2MgSiO_4 and B_2O_3, MgF_2, WO_3 added Li_2MgSiO_4 for substrate applications, Appl. Surf. Sci. 449 (2018) 96–104.
[33] R. Peng, Y.X. Li, X.L. Tang, et al., Improved sintering and microwave dielectric properties of Li_2CaSiO_4 ceramic with magnesium atom substitution, Ceram. Int. 46 (7) (2020) 8869–8876.
[34] Y. Tang, M.Y. Xu, L. Duan, et al., Structure, microwave dielectric properties, and infrared reflectivity spectrum of olivine type Ca_2GeO_4 ceramic, J. Eur. Ceram. Soc. 39 (7) (2019) 2354–2359.
[35] C.C. Li, H.C. Xiang, M.Y. Xu, et al., Li_2AGeO_4 (A= Zn, Mg): two novel low-permittivity microwave dielectric ceramics with olivine structure, J. Eur. Ceram. Soc. 38 (4) (2018) 1524–1528.
[36] H. Ohsato, I. Kagomiya, M. Terada, et al., Origin of improvement of Q based on high symmetry accompanying Si-Al disordering in cordierite millimeter-wave ceramics, J. Eur. Ceram. Soc. 30 (2010) 315–318.
[37] W.C. Lou, K.X. Song, F. Hussain, et al., Microwave dielectric properties of $Mg_{1.8}R_{0.2}Al_4Si_5O_{18}$ (R= Mg, Ca, Sr, Ba, Mn, Co, Ni, Cu, Zn) cordierite ceramics and their application for 5G microstrip patch antenna, J. Eur. Ceram. Soc. 42 (5) (2022) 2254–2260.
[38] I. Hameed, L. Li, X.Q. Liu, et al., Ultra-low loss $(Mg_{1-x}Ca_x)_2SiO_4$ dielectric ceramics (x= 0 to 0.15) for millimeter wave applications, J. Am. Ceram. Soc. 105 (3) (2022) 2010–2019.
[39] K.X. Song, P. Liu, H.X. Lin, et al., Symmetry of hexagonal ring and microwave dielectric properties of $(Mg_{1-x}Ln_x)_2Al_4SiO_{18+x}$ (Ln = La, Sm) cordierite-type ceramics, J. Eur. Ceram. Soc. 36 (5) (2016) 1167–1175.
[40] S. Wu, K.X. Song, P. Liu, et al., Effect of TiO_2 doping on the structure and microwave dielectric properties of cordierite ceramics, J. Am. Ceram. Soc. 98.6 (2015) 1842–1847.
[41] Y.P. Pu, Q.W. Zhang, R. Li, et al., Dielectric properties and electrocaloric effect of high-entropy $(Na_{0.2}Bi_{0.2}Ba_{0.2}Sr_{0.2}Ca_{0.2})TiO_3$ ceramic, Appl. Phys. Lett. 115 (22) (2019) 223901.
[42] Y.C. Liu, D.C. Jia, Y. Zhou, et al., $Zn_{0.1}Ca_{0.1}Sr_{0.4}Ba_{0.4}ZrO_3$: a non-equimolar multicomponent perovskite ceramic with low thermal conductivity, J. Eur. Ceram. Soc. 40 (15) (2020) 6272–6277.
[43] Z.B. An, S.C. Mao, Y.N. Liu, et al., A novel HfNbTaTiV high-entropy alloy of superior mechanical properties designed on the principle of maximum lattice distortion, J. Mater. Sci. 79 (2021) 109–117.